Analyzing Characteristics and Distribution of Landslide Triggered By the 2018 Eastern Iburi Earthquake, Hokkaido

Rasis Putra RITONGA, Hefryan Sukma KHARISMALATRI, Takashi GOMI,
Ingrid Ferreira LIMA, Yoshiharu ISHIKAWA
(Tokyo University of Agriculture and Technology)

1. INTRODUCTION

Thousands of shallow landslides were triggered over 400 km^2 area due to Mw 6.7 Eastern Iburi Earthquake on September 18, 2018, Hokkaido, Japan. Most of the landslides collapsed over the air-fall pumice and ash layers part (Yamagishi and Yamazaki 2018). The landslides mass rushed down the steep slopes and deposited in the valley, resulting in 36 fatalities and substantial damage to 192 houses, agriculture facilities, and infrastructures.

Numerous studies had been conducted to investigate the characteristics of earthquake triggered landslide around the world. For instance, Zhou et al. (2016) investigated that landslides occur in mountainous area with elevation range of 800-3000 m and landslide abundance on the elevation of 900-1300 m in 2014 Ludian earthquake in China. By studying the Gorkha earthquake in Nepal, Roback et al. (2018) identified that earthquake triggered landslides occurred in elevation range of 1000-5000 m, resulting in high sediment yields (0.1 to 1.1 km^3) from high elevations range from 2500 to 4000 m.

Various studies also investigated distribution and spatial patterns of landslides. In Chi-Chi earthquake of Taiwan, Wang et al. (2002) showed that mean of landslide density became 10 landslides/km^2 with total landslides number of 1000 landslides over 3750 km^2 of area. On the other hand, Dai et al. (2011) showed that landslide density of Wenchuan earthquake in China was 1.3 landslides/km^2 with total number of 56000 landslides covering an area of 811 km^2. Chen et al. (2014) examined 1000 landslides in a total area of 2200 km^2 of the Lushan earthquake in China and they found that the landslide density was 0.5 landslides/km^2.

Compared to previous studies, Eastern Iburi earthquake is unique in terms of the landslides occurrence and concentration. First, numerous landslides occurred in area with rather gentle and hilly topography (<500 m). Second, landslide was highly concentrated in some specific areas. The density of landslides in Eastern Iburi earthquake was possibly 20 times greater than those by Wenchuan earthquake (Yamagishi and Yamazaki 2018). Such unique characteristics may affect the sediment production and downstream transports. Analyzing the unique characteristics of Eastern Iburi earthquake induced landslide is essential for identifying the worst affected area. This is crucial to set the priority area for sediment management and control in the disaster recovery process. Therefore, the objective of this study is to analyze the characteristics and spatial distribution of landslides induced by the 2018 Eastern Iburi Earthquake, Hokkaido.

2. STUDY AREA AND METHODOLOGY

This study focused on three watersheds with total area of 18.87 km^2. This area was located 10 km to northwest from epicenter. Mean annual precipitation and air temperature are 158 mm and 21.5°C, respectively. The underlain geology materials of this area are Neogene mudstone, sandstone, and conglomerate. Soil depth is approximately 4 m consist of various volcanic deposits such as tephra originated from Mount Tarumae and andosol. The most dominant land use consisted of broad leaved and coniferous forest and agriculture area (e.g., paddy field).

We used LiDAR datasets with 0.5 m resolution and Ortho-photo image with 0.2 m resolution taken on 11th September 2018. We delineated landslide scar and deposition separately using Ortho-photo image. Then, each landslide boundary was assessed using *Minimum Geometry Boundaries* tool from ArcMap ver. 10.3 (Niculita, 2015). Width, length, and length-width ratio were measured as the index of landslide shape. We also used a 0.5 m DEM data to analyze the topographical characteristics of individual landslide including elevation, slope gradient, aspect, and curvature. The landslide position consisted of distance to ridge, stream, and epicenter were analyzed using *Near* tool from ArcMap (Zhuang et al. 2018).

3. RESULTS AND DISCUSSIONS

(1) Geomorphologic characteristics

792 landslide scars in 18.87 km^2 was identified (Fig. 1). 98% of landslides has area <0.015 km^2 while the greatest landslides area was 0.023 km^2. Landslide area of 0.015 km^2 to 0.03 km^2 was the most frequently occurred (29.7%). Based on the ratio of length and width (L/W ratio), 74% of landslides had 1 to 3 of L/W ratio with 1.8 of mean value. Our findings of L/W ratio tended to be smaller than previous studies by Xu and Xu (2014) in Mw 6.9 Yushu earthquake, China. The topographic relief in Yushu earthquake induced landslide (elevation ranges up to 3500 to 5000 m) was much higher than our study (<500 m). Such condition caused greater gravitational potential energy which affected the shape of landslides and potential mobility of the landslides. Other than topographic relief, previous study also pointed out that larger earthquake magnitude may cause larger L/W ratio which resulting in higher mobility of the landslides (Tian et al. 2017).

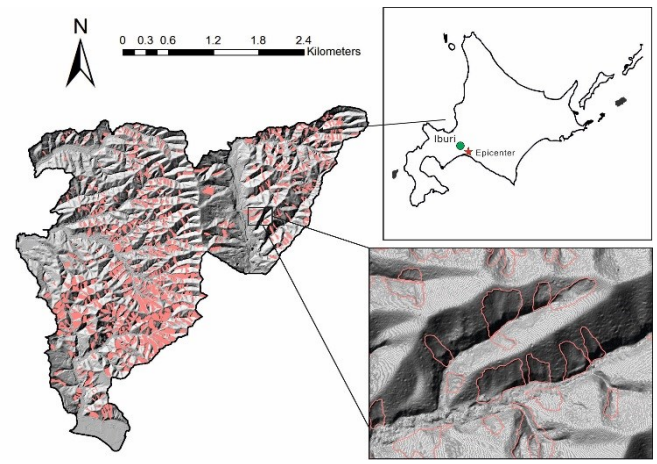

Fig 1. Study area and identified landslides in Iburi Sub Prefecture

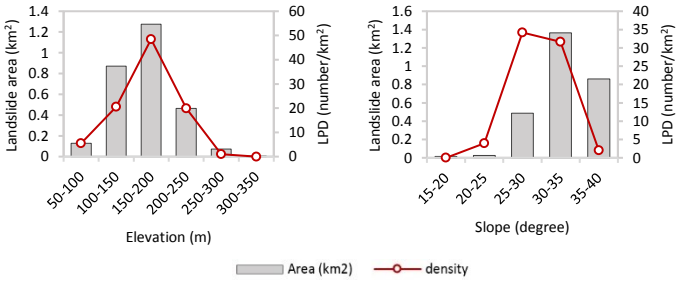

(a) **(b)**

Fig 2. LPD values and area versus topographic factors. **a** Elevation; **b** slope gradient

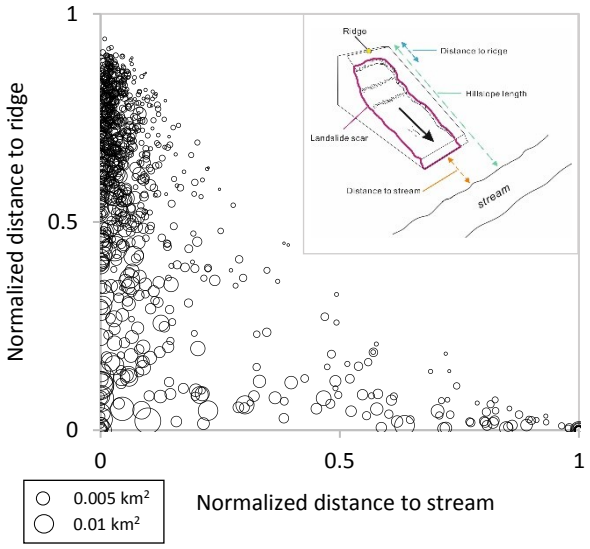

Fig 3. Normalized distance to ridge and stream

(2) Spatial distributions

The Landslides Point Density (LPD) was examined based on the landslides number per square kilometers in given areas of elevation, slope gradient, and slope aspect. LPD value was the highest in elevation of 150 to 200 m, possibly because of high concentration of landslides at near the ridge crest (Fig. 2a). Further, LPD value was high on slope gradient range of 25-35° (Fig. 2b). However, slope gradient >35° generated larger landslide area. In contrast, a study on 2010 Port-au-Prince earthquake induced landslides in Haiti showed that LPD abundance was found in slope gradient of 40-45° (Xu et al. 2014). The landslide area in their study tended to decrease when the slope gradient >45°. Such difference possibly due to the slope in Eastern Iburi area is dominated by 25° to 35° (moderately steep slope area). Furthermore, landslides in our area were concentrated on slope aspect in the direction of Southeast to South. Because our study area located northwest from epicenter, the slope facing the epicenter tends to collapse due to tensile stress called "*back slope effect*" (Zhuang et al. 2018).

Relationship between normalized distance to stream and ridge line indicates the locations of landslide occurrence on the hillslope. (Fig. 3). 54% of the landslide clustered near the ridge (normalized distance to ridge >0.6), followed by near the stream and ridge (17.5%), and near the stream (7%). Meanwhile, the largest landslide area was found in those occurred near ridge and stream, followed by near the stream and near the ridge for 0.006 km^2, 0.003 km^2, and 0.002 km^2 respectively. This result suggested that the upper part of the slope which has steeper slope gradient is more susceptible to landslide with smaller landslide area. Contrastingly, landslides triggered by Jiuzhaigou earthquake in China mostly occurred on the lower part of the slope (Fan et al. 2018). This dissimilarity possibly because of different hillslope morphology among the study areas. The hillslope in Jiuzhaigou earthquake has steep slope gradient on lower part near the stream, while the hillslope in Eastern Iburi earthquake dominantly steep near the ridge crest.

4. CONCLUSIONS

Based on our findings, the characteristics and distributions are very important to recognize the location of landslide affected area over broad region in more efficient way. Furthermore, the proper mitigation planning can be arranged in assessing the highest priority location that needs to be concerned after the landslides occurrence by the earthquake. For further investigation, we will estimate the volume of the landslides to propose the most effective counter measured needed to be developed in sediment controls management after the earthquake.

5. REFERENCES

Chen XL, Yu L, Li JY, Liu CG, Lin CX, Wang, MM. 2014. Brief Communication: Landslides triggered by the 7.0 Lushan earthquake, China. Natural Hazards and Earth System Sciences 14(5): 1257–1267

Dai FC, Xu C, Yao X, Xu L, Tu XB, & Gong QM. 2011. Spatial distribution of landslides triggered by the 2008 Ms 8.0 Wenchuan earthquake, China. Journal of Asian Earth Sciences 40(4): 883–895.

Fan X, Scaringi G, Xu Q, Zhan W, Dai L, Li Y, Huang R. 2018. Coseismic landslides triggered by the 8th August 2017 M_s 7.0 Jiuzhaigou earthquake (Sichuan, China): factors controlling their spatial distribution and implications for the seismogenic blind fault identification. Landslides 15(5): 967–983.

Niculita M. 2015. Automatic extraction of landslide flow direction using geometric processing and DEMs. Geomorphometry 201–203.

Roback K, Godt JW, Clark MK, Li G, Gallen SF, Zekkos D, Chamlagain D. 2017. The size, distribution, and mobility of landslides caused by the 2015 Mw7.8 Gorkha earthquake, Nepal. Geomorphology 301: 121–138.

Tian Y, Xu C, Chen J, Zhou Q, Shen L. 2017. Geometrical characteristics of earthquake-induced landslides and correlations with control factors: a case study of the 2013 Minxian, Gansu, China, Mw 5.9 event. Landslides 14(6): 1915–1927.

Wang WN, Nakamura H, Tsuchiya S, & Chen CC. 2012. Distributions of landslides triggered by the Chi-chi Earthquake in Central Taiwan on September 21, 1999. Landslides 38(4): 318–326.

Xu C, Xu X. 2014. Statistical analysis of landslides caused by the Mw 6.9 Yushu, China, earthquake of April 14, 2010. Natural Hazards 72(2): 871–893.

Xu C, Shyu JBH, & Xu X. 2014. Landslides triggered by the 12 January 2010 Port-au-Prince, Haiti, Mw = 7.0 earthquake: Visual interpretation, inventory compiling, and spatial distribution statistical analysis. Natural Hazards and Earth System Sciences 14(7): 1789–1818.

Yamagishi H, Yamazaki F. 2018. Landslides by the 2018 Hokkaido Iburi-Tobu Earthquake on September 6. Landslides 15(12): 2521–2524.

Zhou S, Chen G, & Fang L. 2016. Distribution pattern of landslides triggered by the 2014 Ludian Earthquake of China: implications for regional threshold topography and the seismogenic fault Identification. ISPRS International Journal of Geo-Information *5*(4): 46.

Zhuang J, Peng J, Xu C, Li Z, Densmore A, Milledge D, Cui Y. 2018. Distribution and characteristics of loess landslides triggered by the 1920 Haiyuan Earthquake, Northwest of China. Geomorphology 314: 1–12.

Keyword: *Landslide, Earthquake, LiDAR, Topographic Characteristics, GIS*